Spin-resolved charge displacement analysis as an intuitive tool for the evaluation of cPCET and HAT scenarios

D'Amore, Lorenzo; Belpassi, Leonardo; Klein, Johannes E. M. N.; Swart, Marcel

Published in:
Chemical Communications

DOI:
10.1039/d0cc04995f

ChemComm

COMMUNICATION

View Article Online
View Journal | View Issue

Cite this: *Chem. Commun.*, 2020, **56**, 12146

Received 21st July 2020,
Accepted 4th September 2020

DOI: 10.1039/d0cc04995f

rsc.li/chemcomm

Spin-resolved charge displacement analysis as an intuitive tool for the evaluation of cPCET and HAT scenarios†

Lorenzo D'Amore, [a] Leonardo Belpassi, [b] Johannes E. M. N. Klein [c] and Marcel Swart *[ad]

We introduce here the spin-resolved version of the charge displacement function, which is applied to two competing pathways of proton-coupled electron transfer in oxidation catalysis (hydrogen-atom transfer, concerted proton-coupled electron transfer). The difference in charge displacement between the two mechanisms is directly observable and can be translated to electron flow using this new analysis tool.

Proton-coupled electron transfer (PCET)[1–5] is a ubiquitous process in chemistry and biology, covering areas such as oxidation catalysis,[6] enzymatic reactions[7,8] and photosynthesis.[9–12] The PCET concept is used ambiguously in any process involving the movement of a proton and an electron.[2] However, in the literature the use of the term PCET is far from consistent, following different definitions that depend on whether the proton and the electron move together in space (same or different endpoint) and time (synchronous or sequentially). Indeed, a useful general guidance is to distinguish between (i) the stepwise mechanism where the electron transfer (ET) and the proton transfer (PT) take place in a sequential manner, and (ii) concerted PCET (cPCET)[13] in which the proton and the electron are transferred simultaneously. A variant of the latter are reactions where the proton and the electron are transferred together, which is best described as the transfer of a genuine hydrogen atom (radical), which are usually denoted hydrogen atom transfer (HAT) reactions. Scheme 1 offers an overview of these representative cases.

The operation of a stepwise or a concerted mechanism can be inferred by the presence of a discrete intermediate that can in some cases even be isolated experimentally. However, such a rigorous distinction between stepwise and concerted is not always straightforward, as it may relate back to the arbitrary definition of a lifetime (of an intermediate), which in turn may depend on the (choice of) experimental apparatus.[5] Because of this, the Hammes-Schiffer group has developed a protocol to distinguish cPCET from HAT, based on the electron-proton nonadiabaticity, which reflects the change in the charge distribution taking place during the reaction.[14–16] Nevertheless, the interplay between experimental and theoretical methods is often still required or useful,[5] making this rather a complex procedure to apply where often chemical intuition is not appealed to directly.

Other methods have also been proposed, *e.g.* based on the evaluation of the deformation energies at the transition state (TS) of the active complex,[6] the screening of chemical descriptors resulting from multireference calculations[17] or the analysis of the intrinsic bond orbitals (IBOs) along the reaction

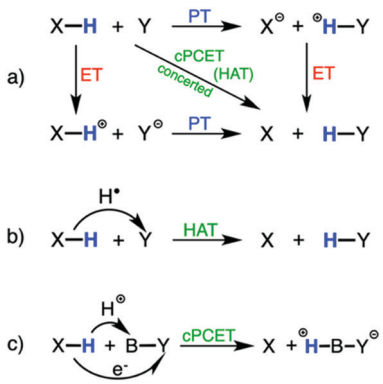

Scheme 1 (a) Concerted *vs.* stepwise CPET mechanism. (b) Hydrogen atom transfer (HAT). (c) Concerted proton-couplet electron transfer (cPCET).

[a] *IQCC and Dept. Chem., Universitat de Girona, Campus Montilivi, 17003 Girona, Spain*
[b] *Istituto di Scienze e Tecnologie Chimiche del CNR (SCITEC-CNR) c/o Università degli Studi di Perugia, Via Elce di Sotto 8, 06123 Perugia, Italy*
[c] *Molecular Inorganic Chemistry, Stratingh Institute for Chemistry, Faculty of Science and Engineering, University of Groningen, Nijenborgh 4, 9747AG, Groningen, The Netherlands*
[d] *ICREA, Pg. Lluis Companys 23, 08010 Barcelona, Spain. E-mail: marcel.swart@gmail.com*

† Electronic supplementary information (ESI) available. See DOI: 10.1039/d0cc04995f

pathway.[18,19] The latter tool shows interesting results, which is intriguing because despite the simplicity, it identified very effectively whether a cPCET or HAT mechanism is operating, by displaying the electron flow occurring upon bond reorganization along the reaction coordinate.

In this paper, we propose an alternative approach which relies on the analysis of the charge displacement function (CDF)[20] that accompanies the formation of a new chemical bond, in terms of the electron density rearrangement that is taking place during the generation of an adduct from two constituting fragments (see below and ESI† Section I.2 for more details). As any PCET event is governed by a significant charge rearrangement this approach addresses the underlying changes to the electronic structure directly and should provide an intuitive way of interpreting results.

In particular, the charge displacement function, $\Delta q(z)$, measures at each point z along a chosen axis (typically chosen along the bond(s) to be formed) the amount of electrons that move across a plane perpendicular to this axis passing through z (see *e.g.* Fig. 1b); this flow of electrons is based on the difference between the final density of the total system and the sum of fragment densities (see ESI† Section I.2 for details). Positive values of $\Delta q(z)$ correspond to electrons flowing in the direction of decreasing z, and negative values to electrons moving to increasing z. Furthermore, a positive slope indicates regions of charge accumulation, and *vice versa* a negative slope indicates depletion.[20] The CDF analysis has been widely applied in closed-shell systems to study *e.g.* charge transfer (CT) contribution in weak interactions[21–26] or the π coordination/activation by gold complexes.[27–30]

Here, we apply open-shell CDF (osCDF) for the first time, using unrestricted Density Functional Theory (DFT), and show that it can successfully discriminate between cPCET and HAT in a chemically intuitive way. To this end, we use the same case studies investigated before using IBOs,[19] involving model systems for the well-studied reactions of lipoxygenase[8,16] and the intermediate TauD-*J*[31–36] of taurine dioxygenase. The active species in lipoxygenase is an Fe(III)–OH, and for TauD-*J* an Fe(IV)–oxo, which cleave C(sp^3)–H bonds with cPCET and HAT mechanisms, respectively. For the sake of consistency, we applied osCDF directly on the TS coordinates available for the two model systems:[19] (i) a high-spin (S = 5/2) Fe^{III}–OH moiety coordinated to an amide, a carboxylate and three imidazoles, with a 2,5-diene as substrate to model the cPCET reaction of lipoxygenase; and (ii) a high-spin (S = 2) Fe^{IV}=O moiety coordinating to two imidazoles and a carboxylate (facial triad[37]) with an acetate to mimic the decarboxylated α-ketoglutarate coordination environment, and ethane as substrate to model the HAT reaction of the TauD-*J* intermediate (see ESI† Section II.1 for a detailed description of the model complexes). We employed the S12g functional[38,39] in combination with a TZ2P basis set (see ESI† Section I.1 for the complete computational details), which was previously demonstrated to provide a consistent description of the spin state and electronic structure in transition-metal complexes.[40–42]

Both systems were represented by (i) the $[Fe(O/OH)(L)]^{0/+}$ complex and (ii) the substrate, as the two fragments for osCDF. The z-axis was chosen to lie along the Fe=O/Fe–O(H) bond, with the O atom at z = 0 and the iron complex at negative z. We start with the HAT mechanism in TauD-*J*, which can be considered as the simpler case.

When the C–H bond is cleaved *via* HAT, it is generally accepted[36] that the $^5\sigma$-channel represents the most favorable pathway (see ESI† Section II.2), where the α-spin electron moves from the C–H bond to the σ* (Fe dz^2–O p_z) antibonding orbital of the Fe=O unit to form the new O–H bond, whereas the other electron proceeds from the β-spin manifold of the :O(Fe) lone pair, as depicted in Scheme 2. Fig. 1a shows the 3D contour plots of how the α/β/total electron density changes when the fragments are brought together from infinite separation to the structure they attain at the TS.

Note that the positions of the H, C and O atom involved in the HAT are explicitly indicated in Fig. 1a (left), and in the ESI†

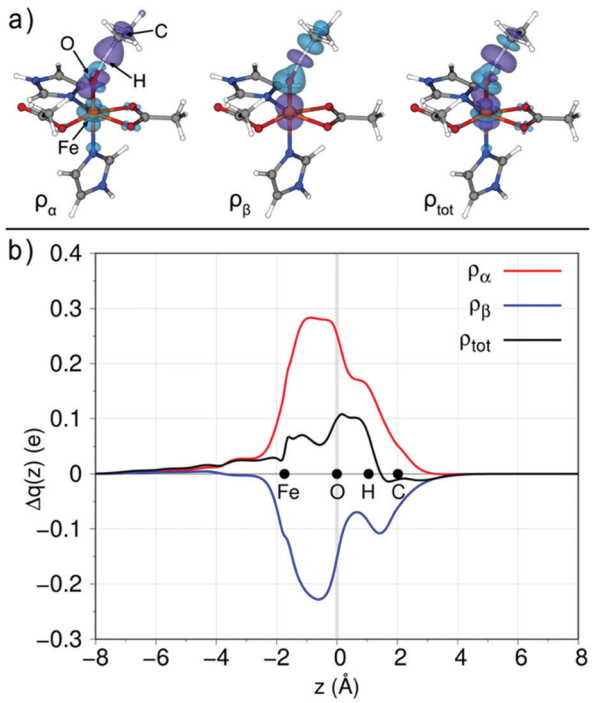

Fig. 1 3D contour plots (± 0.035 e au^{-3}) of the $\Delta\rho$ for the FeO–H(substrate) bond in the TS of the TauD-*J* model complex: (a) α, β and total spin-density, cyan (violet) ribbon color corresponds to regions of charge accumulation (depletion); (b) CD curves of the corresponding density differences in (a). Red, blue and black curves corresponds to α, β and total density, respectively.

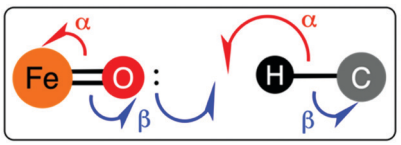

Scheme 2 Representation of the electron flow in the HAT mechanism from C(sp^3)–H bond to the Fe^{IV}=O acceptor of the TauD-*J* intermediate. α- and β-spin electrons are drawn with red and blue arrows, respectively.

(Section II.3) we present an alternative view where we have rotated the system to highlight the changes around these three atoms. It is interesting to see (Fig. 1a) a substantial decrease of α-spin density (σ-shaped) in the C–H region with a less pronounced increase in the O–H region, which is accompanied by a simultaneous charge rearrangement in the Fe=O unit: a decrease in the O(p_z)-shaped α-density is noticed, with a concurrent increase in the Fe(d_{z^2})-shaped α-density. On the other hand, the β-spin difference shows the rearrangement of the Fe=O unit with a shift from Fe(p_z) to the O–H moiety. It is accompanied by a decrease of β-density in the H atom region and an increase around the C atom, consistent with Scheme 2.

The total electron density difference 3D contour plots is also shown in Fig. 1a. Here, a substantial depletion from the C–H region with a concomitant increase in the O–H region can be appreciated, concurrently with a decrease in the Fe–O bond and a slight accumulation on the Fe atom. The osCDF plot (Fig. 1b) finally gives us a quantitative picture of the charge fluxes associated with α-, β- and total-density rearrangement as discussed above. The osCDF associated with the α-density rearrangement is found to be positive in the whole molecular region (red curve), thus unambiguously indicating a net charge flux from the right to the left in the direction going from the C(sp^3)–H bond to the Fe^{IV}=O acceptor. On the contrary, the osCDF associated to the β-spin polarization (blue curve) is negative and the associated charge flux goes in the opposite direction. Noteworthy, for instance, if we evaluate the CDFs in the region of the Fe–O bond we can easily quantify that about 0.28 electrons of β-spin accumulate at the Fe site while about the same amount of charge (0.22 *e*) of opposite spin polarization (α-spin) moves from the same region. This can be interpreted as the swapping of an β-electron on Fe with an α-electron, where the β-electron moves onto OH, anti-ferromagnetically coupled to Fe^{III} in an exchange-coupled Fe^{III}–OH system.[19]

We now move to the cPCET reaction of lipoxygenase, following the same scheme as before. In this case, the d-shell manifold of the Fe–OH complex is fully occupied with 5 electrons of α-spin, so that a β-electron is transferred from the σ C–H bond to the π* (Fe $d_{xz/yz}$–O $p_{x/y}$) antibonding orbital of the Fe–OH unit *via* a ^{6}π-channel (see ESI† Section II.2). However, typical for PCET events, this time the β-electron from the cleaved C–H bond populates the metal-based d-orbitals, whereas the newly formed O–H bond is created with both electrons proceeding from the :OH(Fe) lone pair, as depicted in Scheme 3.

The α-spin contour plot (Fig. 2a) shows a decrease of α-density on oxygen and an increase in the O–H region of the newly formed bond; simultaneously, α-density is moving within the CH-moiety from the hydrogen to carbon; a small depletion of α-electron on Fe is also appreciable (see ESI† Section II.4 for an alternative view, highlighting the changes in the O···H···C region). For the change in β-spin density generally we note an accumulation on the O atom with effectively depletion on oxygen itself to form a lobe in the direction of the to-be formed O–H bond, resulting in an accumulation in the O–H region. A substantial decrease of β-spin density (σ-shaped) in the C–H region is present, together with an accumulation on Fe resembling a $d_{xz/yz}$ shaped orbital. However, a certain amount of β-spin density depletion is also noticeable around Fe. It should be noted that a depletion at oxygen in both the α- and β-spin density was not present in the TauD-*J* intermediate; this is a clear indication that in lipoxygenase both the α- and β-spin electrons are transferred to form the new O–H bond. Overall, in the total spin density difference, we note on the O atom a lobe of accumulating charge density pointing towards the to-be formed O–H bond, with a consequent increase at the O–H region. It is accompanied by a significant decrease in density on the transferring H atom, coupled with an accumulation on the C atom of the substrate. The total density accumulated and depleted on the iron is mainly coming from the β-spin density in Fig. 2a, since the change in α-spin density on iron was negligible. The flow of electrons in lipoxygenase therefore is consistent with the arrows of Scheme 3.

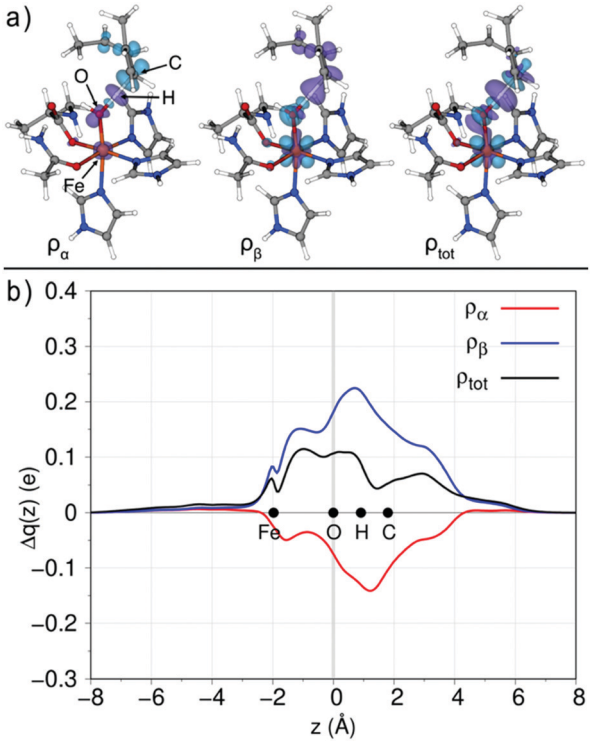

Fig. 2 3D contour plots (±0.035 e au^{-3}) of the $\Delta\rho$ for the FeO–H(substrate) bond in the TS of the lipoxygenase model complex: (a) α, β and total spin-density, cyan (violet) ribbon color corresponds to regions of charge accumulation (depletion); (b) CD curves of the corresponding density differences in (a). Red, blue and black curves corresponds to α, β and total spin-density, respectively.

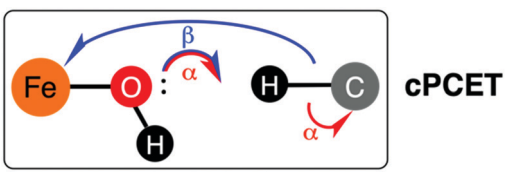

Scheme 3 Representation of the electron flow in the cPCET mechanism from C(sp^3)–H bond to the Fe^{III}–OH acceptor of lipoxygenase. α- and β-spin electrons are drawn with red and blue arrows, respectively.

The difference between the HAT mechanism of TauD-*J* (Fig. 1b) and the cPCET mechanism of lipoxygenase (Fig. 2b) is easily seen by focusing on the Fe–O and C–H regions. In the HAT mechanism, as already mentioned, the α-flow from the oxygen to the iron is accompanied by a β-flow in the opposite direction, and of approximately the same magnitude. For cPCET however, across the Fe–O unit there is only a β-flow (about 0.15 *e*) towards iron and hardly an α-flow (below 0.04 *e*) in the opposite direction. Overall, a net gain of charge density in the Fe–O region is only observed for cPCET, but not for HAT, which would be consistent with the expected flow of electrons (Schemes 2 and 3) for these two mechanisms. Furthermore, by using an alternative view that focuses in particular on the C–H region (ESI† Sections II.3/II.4), one immediately observes the differences between depletion only (α-flow for TauD-*J*, β-flow for lipoxygenase) *vs.* depletion around H together with accumulation around C (β-flow for TauD-*J*, α-flow for lipoxygenase). Moreover, the overall slope of the osCDF (ESI† Section II.5) shows the breaking of the C–H bond with electrons flowing to the left (H, depletion) and right (C, accumulation), fully consistent with chemical intuition.

To summarize, we have applied the open-shell charge displacement function in two well-defined model systems that perform C(sp^3)–H bond cleavage *via* a HAT or cPCET mechanism, showing that this simple and intuitive approach is suited to distinguish the electron flow that takes place during the two different scenarios. By focusing on these two well-understood examples, our study serves as a proof-of-concept for the osCDF for providing an intuitive approach for elucidating the fundamental principles behind this type of reactions, and validating its use for detailed investigations of electron flows in reaction mechanisms and understanding the electronic structure (changes) of more complex systems.

MINECO (CTQ2017-87392-P), FEDER (UNGI10-4E-801), and the Univ. Girona (IFUdG2016 fellowship LD'A) are gratefully thanked for financial support, CSUC for extensive computer time and SCM for a developer's license.

Conflicts of interest

There are no conflicts to declare.

References

1 J. M. Mayer, *Annu. Rev. Phys. Chem.*, 2004, **55**, 363–390.
2 M. H. V. Huynh and T. J. Meyer, *Chem. Rev.*, 2007, **107**, 5004–5064.
3 J. J. Warren, T. A. Tronic and J. M. Mayer, *Chem. Rev.*, 2010, **110**, 6961–7001.
4 D. R. Weinberg, C. J. Gagliardi, J. F. Hull, C. F. Murphy, C. A. Kent, B. C. Westlake, A. Paul, D. H. Ess, D. G. McCafferty and T. J. Meyer, *Chem. Rev.*, 2012, **112**, 4016–4093.
5 S. Hammes-Schiffer, *J. Am. Chem. Soc.*, 2015, **137**, 8860–8871.
6 D. Usharani, D. C. Lacy, A. S. Borovik and S. Shaik, *J. Am. Chem. Soc.*, 2013, **135**, 17090–17104.
7 J. Stubbe, D. G. Nocera, C. S. Yee and M. C. Y. Chang, *Chem. Rev.*, 2003, **103**, 2167–2202.
8 M. J. Knapp, K. Rickert and J. P. Klinman, *J. Am. Chem. Soc.*, 2002, **124**, 3865–3874.
9 C. W. Hoganson and G. T. Babcock, *Science*, 1997, **277**, 1953.
10 A. Magnuson, M. Anderlund, O. Johansson, P. Lindblad, R. Lomoth, T. Polivka, S. Ott, K. Stensjö, S. Styring, V. Sundström and L. Hammarström, *Acc. Chem. Res.*, 2009, **42**, 1899–1909.
11 J. H. Alstrum-Acevedo, M. K. Brennaman and T. J. Meyer, *Inorg. Chem.*, 2005, **44**, 6802–6827.
12 T. J. Meyer, M. H. V. Huynh and H. H. Thorp, *Angew. Chem., Int. Ed.*, 2007, **46**, 5284–5304.
13 Various acronyms find use in the literature for this specific scenario, such as EPT and CPET. Unfortunately, at times simply PCET, the overarching term, is used to describe such scenarios.
14 J. H. Skone, A. V. Soudackov and S. Hammes-Schiffer, *J. Am. Chem. Soc.*, 2006, **128**, 16655–16663.
15 A. Sirjoosingh and S. Hammes-Schiffer, *J. Phys. Chem. A*, 2011, **115**, 2367–2377.
16 A. V. Soudackov and S. Hammes-Schiffer, *J. Phys. Chem. Lett.*, 2014, **5**, 3274–3278.
17 C. A. Gaggioli, J. Sauer and L. Gagliardi, *J. Am. Chem. Soc.*, 2019, **141**, 14603–14611.
18 G. Knizia, *J. Chem. Theory Comput.*, 2013, **9**, 4834–4843.
19 J. E. M. N. Klein and G. Knizia, *Angew. Chem., Int. Ed.*, 2018, **57**, 11913–11917.
20 L. Belpassi, I. Infante, F. Tarantelli and L. Visscher, *J. Am. Chem. Soc.*, 2008, **130**, 1048–1060.
21 F. Pirani, D. Cappelletti, S. Falcinelli, D. Cesario, F. Nunzi, L. Belpassi and F. Tarantelli, *Angew. Chem., Int. Ed.*, 2019, **58**, 4195–4199.
22 F. Nunzi, D. Cesario, L. Belpassi, F. Tarantelli, L. F. Roncaratti, S. Falcinelli, D. Cappelletti and F. Pirani, *Phys. Chem. Chem. Phys.*, 2019, **21**, 7330–7340.
23 F. Nunzi, D. Cesario, F. Pirani, L. Belpassi and F. Tarantelli, *ChemPhysChem*, 2018, **19**, 1476–1485.
24 G. Ciancaleoni and L. Belpassi, *J. Comput. Chem.*, 2020, **41**, 1185–1193.
25 L. Belpassi, M. L. Reca, F. Tarantelli, L. F. Roncaratti, F. Pirani, D. Cappelletti, A. Faure and Y. Scribano, *J. Am. Chem. Soc.*, 2010, **132**, 13046–13058.
26 D. Cappelletti, E. Ronca, L. Belpassi, F. Tarantelli and F. Pirani, *Acc. Chem. Res.*, 2012, **45**, 1571–1580.
27 G. Bistoni, P. Belanzoni, L. Belpassi and F. Tarantelli, *J. Phys. Chem. A*, 2016, **120**, 5239–5247.
28 L. D'Amore, G. Ciancaleoni, L. Belpassi, F. Tarantelli, D. Zuccaccia and P. Belanzoni, *Organometallics*, 2017, **36**, 2364–2376.
29 L. Gregori, D. Sorbelli, L. Belpassi, F. Tarantelli and P. Belanzoni, *Inorg. Chem.*, 2019, **58**, 3115–3129.
30 G. Bistoni, L. Belpassi and F. Tarantelli, *Angew. Chem., Int. Ed.*, 2013, **52**, 11599–11602.
31 C. Krebs, D. Galonić Fujimori, C. T. Walsh and J. M. Bollinger, *Acc. Chem. Res.*, 2007, **40**, 484–492.
32 S. Kal and L. Que, *J. Biol. Inorg. Chem.*, 2017, **22**, 339–365.
33 J. C. Price, E. W. Barr, T. E. Glass, C. Krebs and J. M. Bollinger, *J. Am. Chem. Soc.*, 2003, **125**, 13008–13009.
34 J. M. Bollinger and C. Krebs, *J. Inorg. Biochem.*, 2006, **100**, 586–605.
35 J. M. Bollinger Jr, W.-C. Chang, M. L. Matthews, R. J. Martinie, A. K. Boal and C. Krebs, *2-Oxoglutarate-Dependent Oxygenases*, The Royal Society of Chemistry, 2015, pp. 95–122.
36 S. Ye and F. Neese, *Proc. Natl. Acad. Sci. U. S. A.*, 2011, **108**, 1228–1233.
37 K. D. Koehntop, J. P. Emerson and L. Que, *J. Biol. Inorg. Chem.*, 2005, **10**, 87–93.
38 M. Swart, *Chem. Phys. Lett.*, 2013, **580**, 166–171.
39 M. Swart and M. Gruden, *Acc. Chem. Res.*, 2016, **49**, 2690–2697.
40 S. K. Padamati, D. Angelone, A. Draksharapu, G. Primi, D. J. Martin, M. Tromp, M. Swart and W. R. Browne, *J. Am. Chem. Soc.*, 2017, **139**, 8718–8724.
41 K. Rajabimoghadam, Y. Darwish, U. Bashir, D. Pitman, S. Eichelberger, M. A. Siegler, M. Swart and I. Garcia-Bosch, *J. Am. Chem. Soc.*, 2018, **140**, 16625–16634.
42 S. Banerjee, A. Draksharapu, P. M. Crossland, R. Fan, Y. Guo, M. Swart and L. Que Jr., *J. Am. Chem. Soc.*, 2020, **142**, 4285–4297.